Chemical Science

ROYAL SOCIETY OF CHEMISTRY

EDGE ARTICLE

View Article Online
View Journal | View Issue

Cite this: *Chem. Sci.*, 2026, **17**, 6426

All publication charges for this article have been paid for by the Royal Society of Chemistry

B ← N Lewis pair fusion of [6]helicene: one way to integrate circularly polarized luminescence with two-photon absorption

Min Wang,[ab] Zhi-Qiang Liu *[c] and Cui-Hua Zhao *[a]

It is very challenging to integrate circularly polarized luminescence (CPL) and two-photon absorption (TPA) in a single organic molecule, which is of great interest for advanced optoelectronic and bioimaging applications. We here disclose the synthesis and properties of a new family of helicenes, in which [6]helicene is fused with six-membered B ← N heterocycles. Benefiting from the strong electron-affinity of the B ← N Lewis pair, the introduction of an electron-donating (*para*-diphenylamino)phenyl (*p*-$Ph_2NC_6H_4$) group induces intramolecular charge transfer (CT) characteristics. For mono-fused derivatives, both molar absorption coefficients (ε) and fluorescence quantum yields (Φ_F) progressively increase with enhancement of the intramolecular CT feature through introduction of *p*-$Ph_2NC_6H_4$ and replacement of the boron-bound phenyl group with more electron-withdrawing perfluorophenyl. Moreover, the structural evolution from a mono-fused dipolar to a bis-fused quadrupolar architecture results in more than a twofold increase in ε and simultaneous significant enhancement of the TPA cross section (δ_{TPA}) and luminescence dissymmetry factor (g_{lum}). It thus became possible to achieve integration of excellent CPL and TPA properties in a single molecule for the bis-fused quadrupolar [6]helicene **BiNFBPy-HC**, with δ_{TPA} up to 1361 GM and CPL brightness (B_{CPL}) reaching 13.2 M^{-1} cm^{-1}, owing to its large ε (8.84×10^4 M^{-1} cm^{-1}), good Φ_F (0.41) and moderate $|g_{lum}|$ (7.37×10^{-4}).

Received 8th November 2025
Accepted 23rd January 2026

DOI: 10.1039/d5sc08697c

rsc.li/chemical-science

Introduction

Organic materials exhibiting circularly polarized luminescence (CPL) have gained rapidly increasing attention in the last decade owing to their broad potential applications in 3D displays,[1,2] optical data storage,[3,4] biological probes and signatures.[5,6] An ideal CPL-active material is expected to have not only a high fluorescence quantum yield (Φ_F) but also a high luminescence dissymmetry factor ($g_{lum} = 2(I_L - I_R)/(I_L + I_R)$).[7,8] More recently, CPL brightness ($B_{CPL} = \varepsilon \times \Phi_F \times |g_{lum}|/2$), which also takes the molar extinction coefficient (ε) into account, has emerged as a more comprehensive parameter to evaluate the overall performance of CPL properties.[9] Beyond achieving high B_{CPL}, integrating CPL with additional optical functionalities, in particular, two-photon absorption (TPA), has become an important topic in this field. TPA allows excellent 3D resolution and absorption of lower-energy (near-infrared) light with reduced photodamage and deeper tissue penetration.[10–12] The combination of CPL and TPA in a single molecule would not only lay a solid foundation for two-photon-excited CPL confocal microscopy in bioimaging but also open new avenues for other advanced optoelectronic applications.[13,14] Nevertheless, examples that simultaneously exhibit high B_{CPL} and large TPA cross section (δ_{TPA}) remain extremely rare (Fig. 1a).[15–17] To achieve efficient TPA, one widely adopted strategy is to construct systems featuring intramolecular charge transfer (CT) characteristics by simultaneous incorporation of electron donor (D) and acceptor (A) groups.[18,19] Three typical structures are generally employed, namely dipolar (D–A),[20–22] quadrupolar (D–A–D or A–D–A),[23,24] and octupolar [$D–A_3$ or $A–D_3$] architectures.[25–27] Compared with dipolar systems, the multibranched quadrupoles and octupoles tend to display larger δ_{TPA} values due to the enhanced electron coupling among branches. In this context, it was envisioned that the construction of multipolar chiral systems may provide a promising route to achieve integrated CPL and TPA properties. Probably due to synthesis challenges, such examples have not been explored.

Helicenes, characterized by an extended π-conjugation structure and inherent helical chirality, have long been recognized as promising skeletons for CPL-active molecules.[28–30] However, parent helicenes suffer from very low Φ_F values (Φ_F < 0.05 for [*n*]helicenes, $n \geq 5$), primarily due to the fast intersystem crossing (ISC) process.[31,32] Herein, considerable efforts have been devoted to increasing Φ_F of helicenes. One efficient strategy is to incorporate heteroatoms into helicene frameworks

[a]*School of Chemistry and Chemical Engineering, Shandong University, Jinan 250100, China. E-mail: chzhao@sdu.edu.cn*

[b]*Shandong Engineering Research Center of New Energy Materials and Devices, Weifang University of Science and Technology, Weifang 262700, China*

[c]*State Key Laboratory of Crystal Materials, Shandong University, Jinan 250100, China. E-mail: zqliu@sdu.edu.cn*

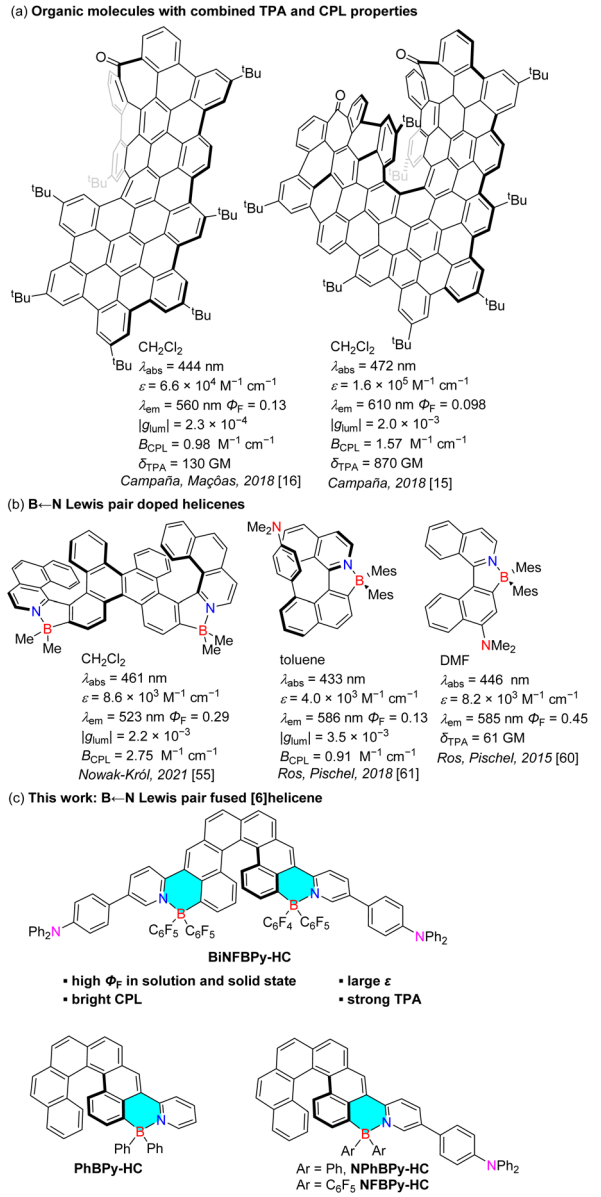

Fig. 1 (a) Examples of small organic molecules with combined TPA and CPL properties. (b) Examples of reported B ← N Lewis pair doped helicenes. (c) Chemical structure of B ← N Lewis pair-fused [6] helicenes in this work.

to perturb electronic structures.[33–42] Another is to enlarge π-conjugation by fusion with polycyclic arenes or attachment of peripheral substituents.[43–49] For the first strategy, one representative approach is to replace C=C bonds with their isoelectronic B–N couple counterparts, which are typically formed *via* N-directed borylative cyclization of amino precursors.[40–42] Instead of embedding the B–N couple into the parent helicene backbone, we have recently prepared B–N heterocycle-fused [6]helicenes using *ortho*-phenylamine-substituted precursors.[50] It was found that the fusion with the B–N heterocycle helps extend π-conjugation and increase both the absorptivity and fluorescence efficiency of the first excited state.

Remarkably, a double [6]helicene derivative can show outstanding CPL performance with B_{CPL} reaching 49.0 M^{-1} cm^{-1}, owing to its very high Φ_F (0.87), large ε (5.47 × 10^4 M^{-1} cm^{-1}), and fairly good $|g_{lum}|$ (2.06 × 10^{-3}).

Inspired by the outstanding CPL performance of B–N heterocycle-fused [6]helicenes, we turned our attention to helicenes fused with heterocycles containing a B ← N Lewis pair, which remain unprecedented to date. Similar to the covalent B–N bond, intramolecular B ← N coordination bond formation can planarize and rigidify π-systems,[51–53] thereby suppressing the nonradiative decay process and boosting Φ_F, which have been well demonstrated by a number of highly emissive B ← N-doped helicenes (Fig. 1b).[54–61] Moreover, the B ← N unit tends to increase the electron affinity of the system,[62–64] which can endow the systems with intramolecular CT characteristics and thereby TPA properties when electron-donor groups are also introduced.[60,61] Considering the facile accessibility of 5,12-dibromo[6]helicene and its easy transformation into a donor-substituted 2-pyridyl derivative, we envisioned that it was possible to prepare a quadrupole B ← N Lewis pair-fused [6]helicene. Following this strategy, we successfully synthesized a bis-B ← N Lewis pair-fused [6]helicene, **BiNFBPy-HC** (Fig. 1c), in which a strong electron-donating (*para*-diphenylamino)phenyl (*p*-$Ph_2NC_6H_4$) group was introduced at the 4-position of the 2-pyridyl unit. It was fascinating to find that this molecule exhibits both excellent CPL and TPA properties with B_{CPL} up to 13.2 M^{-1} cm^{-1} and δ_{TPA} up to 1361 GM. To further probe the influence of B ← N Lewis pair fusion and structural modification on photophysical properties, we also synthesized mono-fused derivatives, **PhBPy-HC**, **NPhBPy-HC**, and **NFBPy-HC**, which differ in the presence of electron donor groups and the substituent at the boron center. Herein, we report detailed results on the synthesis, structures and fascinating properties of these unprecedented B ← N Lewis pair-fused [6]helicenes.

Results and discussion

Synthesis and structures

The synthetic routes to the B ← N Lewis pair-fused [6]helicenes are depicted in Scheme 1. A typical method for the synthesis of stable B ← N Lewis pairs is N-directed electrophilic borylative cyclization, followed by trapping of the dihaloborane intermediate with organometallic reagents.[65] Thus, the key point of the synthesis is the preparation of 2-pyridyl-substituted [6]helicene precursors. The precursor to **PhBPy-HC**, 5-(2-pyridyl)[6]helicene (**Py-HC**), was readily synthesized *via* a Pd-catalyzed Suzuki cross-coupling of 2-bromopyridine (**Br-Py**) with [6]helicene-5-boronic ester (**BPin-HC**), which we had previously prepared.[50] To access 5-{5-[4-(*N*,*N*-diphenylamino)phenyl]-2-pyridyl}helicene (**NPy-HC**), the precursor for the mono-fused derivatives, **NPhBPy-HC** and **NFBPy-HC**, we initially attempted to adopt a similar Suzuki cross-coupling of **BPin-HC** with 2-bromo-4-[(4-*N*,*N*-diphenylamino) phenyl]pyridine (**BrNPy**), which was conveniently obtained through selective coupling of 2-bromo-5-iodopyridine with [(4-*N*,*N*-diphenylamino)phenyl]boronic acid (Scheme S1). However, challenges arose during the preparation of 5,12-bis{5-[4-(*N*,*N*-

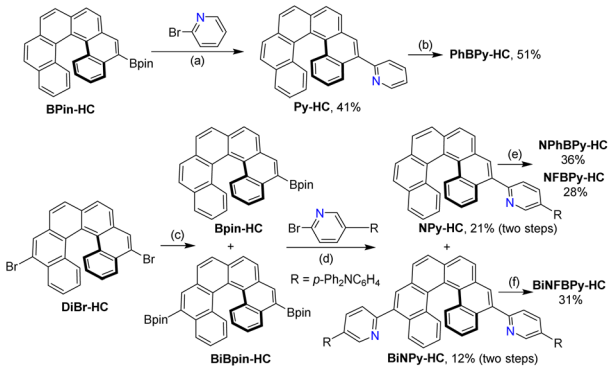

Scheme 1 Synthesis of B ← N Lewis pair-fused [6]helicenes. Reagents and conditions: (a) $PdCl_2$(dppf), K_2CO_3, THF-H_2O, and 80 °C; (b) (i) BBr_3, CH_2Cl_2, *i*-Pr_2NEt, and r.t.; (ii) PhMgBr, toluene, and r.t.; (c) $PdCl_2$(dppf), KOAc, 1,4-dioxane, and 100 °C; (d) Pd_2dba_3, Sphos, K_3PO_4, DMF-H_2O, and 90 °C; (e) (i) BBr_3, CH_2Cl_2, *i*-Pr_2NEt, and 60 °C; (ii) ArMgBr (PhMgBr for **NPhBPy-HC**, C_6F_5MgBr for **NFBPy-HC**), toluene, and r.t.; (f) (i) BBr_3, CH_2Cl_2, *i*-Pr_2NEt, and 60 °C; (ii) C_6F_5MgBr, toluene, and 90 °C.

diphenylamino)phenyl]-2-pyridyl}[6]helicene (**BiNPy-HC**), the precursor for bis-fused **BiNFBPy-HC**. The planned route involved Suzuki coupling of 5,12-dibromo[6]helicene (**DiBr-HC**) with bis(pinacolato)-diboron to afford [6]helicene-5,12-diboronic ester (**BiBPin-HC**) and a second Suzuki coupling of **BiBPin-HC** with **BrNPy**. Unexpectedly, mono-debromination occurred during the borylation of **DiBr-HC**, resulting in the formation of **BPin-HC** along with the desired **BiBPin-HC**. In addition, **BPin-HC** and **BiBPin-HC** could not be separated through the usual purification techniques, such as flash column chromatography and recrystallization. Therefore, the resulting mixture was used directly in the subsequent coupling with **BrNPy**. Based on the comparison of ^{1}H NMR spectra between the mixture and the pure **BPin-HC** (Fig. S1), the molar ratio of **BPin-HC** to **BiBPin-HC** was determined to be about 1 : 1.4. Fortunately, **NPy-HC** and **BiNPy-HC** could be separated by flash column chromatography. Consequently, both **NPy-HC** and **BiNPy-HC** were prepared simultaneously *via* two-step Suzuki coupling starting from **DiBr-HC**. With the 2-pyridyl-substituted [6]helicene precursors in hand, the final B ← N Lewis pair formation was accomplished through N-directed borylative cyclization with boron tribromide (BBr_3) as the boron source and subsequent quenching of the dibromoborane intermediates with the corresponding arylmagnesium bromides.

The chemical structures of all the B ← N fused [6]helicenes were fully characterized by ^{1}H NMR, ^{13}C NMR, and HR-MS. ^{11}B NMR spectra were also characterized except for **NPhBPy-HC**, which has too poor solubility to afford a sufficiently strong signal. The signals observed in the range of −0.64–−4.69 ppm in the ^{11}B NMR spectra confirmed the presence of tetracoordinate boron atoms (Fig. S2). In the ^{1}H NMR spectrum of **PhBPy-HC**, the presence of one singlet signal in the most downfield region ($\delta = 8.68$ ppm) (Fig. S3), which corresponds to the proton at the 6-position of [6]helicene, indicates that the borylative cyclization occurs at the 4-position to form a six-membered ring rather than at the 6-position to generate a five-membered ring. Consistent with this result, two signals, a singlet and a doublet, with a very small coupling constant ($J = 2.0$ Hz) were observed in the ^{1}H NMR spectra of derivatives containing $Ph_2NC_6H_4$ (Fig. S4). The regioselectivity of borylative cyclization is attributed to the conjugative electronic effect of the 2-pyridyl substituent, which renders the 6,14-positions less reactive toward electrophilic substitution. All the final products are stable in air and water and can be purified by silica gel flash chromatography. Notably, the solubility is greatly affected by the substituent on the boron atom. Compounds **PhBPy-HC** and **NPhBPy-HC** bearing Ph groups show poor solubility in various solvents, whereas **NFBPy-HC** and **BiNFBPy-HC** with C_6F_5 substituents are highly soluble in common solvents such as CH_2Cl_2, $CHCl_3$ and THF.

The presence of tetracoordinate boron atoms and the regioselectivity of borylative cyclization to form six-membered rings were further unambiguously confirmed by single-crystal X-ray diffraction analyses (Fig. 2). Single crystals of racemic **PhBPy-HC** and **NFBPy-HC** suitable for X-ray diffraction analysis were obtained by diffusion of hexane (**PhBPy-HC**) or methanol (**NFBPy-HC**) into their $CHCl_3$ solutions. The B–N bond lengths of **PhBPy-HC** and **NFBPy-HC** were determined to be 1.64 Å and 1.62 Å, respectively, indicating strong Lewis pair interactions between the boron center and pyridyl N atom. It was noted that these two compounds adopt similar helical structures with very close dihedral angles (**PhBPy-HC**: 55.4°; **NFBPy-HC**: 57.9°) and centroid–centroid distances (**PhBPy-HC**: 4.43 Å; **NFBPy-HC**: 4.50 Å) between two terminal benzene rings (P1 and P2) in the [6]helicene skeleton. Owing to the formation of a B ← N Lewis pair, the pyridine ring (P4) is fixed with very high coplanarity to the adjacent P2 ring. Notably, the corresponding dihedral in **NFBPy-HC** (9.9°) is slightly smaller than that in **PhBPy-HC** (13.2°). Another difference in the X-ray structures is that the boron center of **NFBPy-HC** essentially lies within the six-membered ring (P3), while it protrudes in **PhBPy-HC**. The corresponding atom-plane distances are 0.11 Å for **NFBPy-HC** and 0.41 Å for **PhBPy-HC**, respectively. These structural differences may indicate more efficient conjugation between the pyridine ring and [6]helicene in **NFBPy-HC**. Regarding the structure of the triarylamine moiety in **NFBPy-HC**, it was noted that the nitrogen center adopts a perfect planar geometry with a sum of ∠C–N–C of 359.9°. In addition, the phenylene ring P5 of $Ph_2NC_6H_4$is only slightly twisted relative to the pyridine ring (P4), indicating efficient electronic coupling between the electron donating amino group and the electron-accepting B ← N unit.

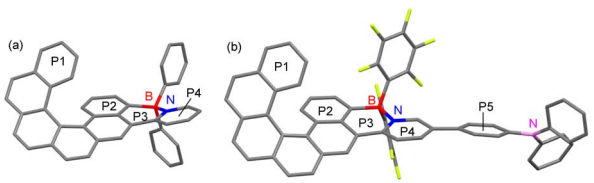

Fig. 2 X-ray crystal structure of (a) **PhBPy-HC** and (b) **NFBPy-HC** (hydrogen atoms are omitted for clarity).

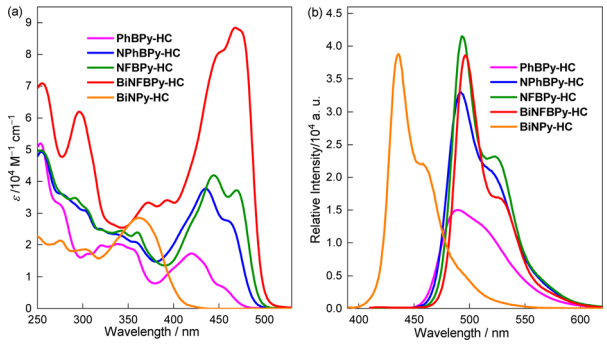

Fig. 3 (a) UV/vis absorption ($c = 2.0 \times 10^{-5}$ M) and (b) fluorescence spectra ($c = 1.0 \times 10^{-5}$ M and $\lambda_{ex} = 400$ nm) of B ← N Lewis pair-fused [6]helicenes in cyclohexane.

Photophysical properties in solutions

The UV-vis absorption and fluorescence spectra of B ← N Lewis pair-fused [6]helicenes are shown in Fig. 3 with the corresponding data summarized in Table 1. In cyclohexane, the mono-B ← N fused [6]helicene **PhBPy-HC** shows the longest absorption at 455 nm, which was observed as a shoulder band and has a moderate intensity ($\varepsilon = 6.8 \times 10^3$ M^{-1} cm^{-1}). The fluorescence maximum is located at 489 nm with a fairly good efficiency ($\Phi_F = 0.25$). Notably, both the longest wavelength absorption and emission of **PhBPy-HC** are much stronger than those of the parent [6]helicene ($\varepsilon = 0.3 \times 10^3$ M^{-1} cm^{-1} and $\Phi_F = 0.05$)[66] and the recently reported mono-BN-naphthalene-fused [6]helicene ($\varepsilon = 1.2 \times 10^3$ M^{-1} cm^{-1} and $\Phi_F = 0.11$).[50] Introducing an electron-donating triphenylamine unit into **NPhBPy-HC** and further replacing the Ph group at the B center with a more electron-withdrawing C_6F_5 in **NFBPy-HC** lead to progressive enhancement of both the longest wavelength absorption and fluorescence intensities. Meanwhile, the longest-wavelength absorption undergoes a red shift to some extent. In contrast, the fluorescence maximum remains almost unchanged, except for the increased prominence of two distinct vibrational bands at 493 and 522 nm ($\Phi_F = 0.49$). The study on excited state dynamics suggests that the gradual increase of Φ_F is mainly ascribed to the acceleration of the radiative decay process. Remarkably, from **NFBPy-HC** to **BiNFBPy-HC**, the further fusion of another B ← N Lewis pair resulted in a substantial increase in absorption intensity, with ε more than doubling to 8.84×10^4 M^{-1} cm^{-1}, while Φ_F slightly decreases to 0.41. Notably, **BiNFBPy-HC** exhibits a very narrow emission band in cyclohexane with a full width at half maximum (FWHM) of only 28 nm, indicating high molecular rigidity and suppressed excited-state structural relaxation. In view of the photophysical properties, another intriguing observation is that **BiNPy-HC**, the precursor of **BiNFBPy-HC**, shows much blue-shifted absorption ($\Delta\lambda = 89$ nm) and fluorescence ($\Delta\lambda = 60$ nm) relative to **BiNFBPy-HC**. In addition, its absorption is much weaker ($\varepsilon = 2.85 \times 10^4$ M^{-1} cm^{-1}) although Φ_F remains nearly unchanged (0.40), highlighting the pronounced role of B ← N coordination in reinforcing absorption intensity. These findings clearly demonstrate that fusing [6]helicene with a B ← N Lewis pair, combined with judicious structural modifications, is effective in achieving intense absorption and strong fluorescence.

Considering the electron affinity of the B ← N Lewis pair and possible intramolecular CT characteristics in these [6]helicene derivatives, we further investigated solvent effects on their absorption and fluorescence (Fig. 4 and Table S4). It was found that the absorption spectra are barely affected by the solvent polarity for all the B ← N Lewis pair-fused [6]helicenes. From nonpolar cyclohexane to polar THF, the observed shifts in the longest wavelength absorption maxima are less than 9 nm, indicating that the electronic structure in the ground state (S_0) is unaffected by the solvent environment. In contrast, the fluorescence solvatochromism is quite different depending on the presence of triphenylamine and the substituent at the boron center. For **PhBPy-HC**, which lacks the electron-donating $Ph_2NC_6H_4$ group, the fluorescence emission remained essentially unchanged from cyclohexane to THF ($\Delta\lambda \leq 3$ nm). However, **NFBPy-HC**, which contains C_6F_5 on B and triphenylamine on the pyridyl ring, exhibited a gradual red-shift in fluorescence from 493 nm in cyclohexane to 553 nm in THF. A more complex fluorescence solvatochromism was observed for **NPhBPy-HC**. From cyclohexane to $CHCl_3$, the shift of fluorescence is minor ($\Delta\lambda = 7$ nm). Interestingly, an abrupt red-shift of 26 nm was observed when the solvent changed from $CHCl_3$ to THF. Notably, the fluorescence maximum of **NFBPy-HC** in THF is 27 nm longer than that of **NPhBPy-HC** although they have nearly identical fluorescence maxima in cyclohexane. Regarding

Table 1 Photophysical property data of B ← N Lewis pair-fused [6]helicenes in cyclohexane and powder form

		λ_{abs}[a]/nm ($\varepsilon/10^4$ M^{-1} cm^{-1})	λ_{em}/nm	Φ_F	$\Delta\nu/10^3$ cm^{-1}	FWHM/nm	τ/ns	$k_r/10^8$ s^{-1}	$k_{nr}/10^8$ s^{-1}
PhBPy-HC	Cyclohexane	419 (1.72), 455 (0.68)	489	0.25[b]	1.53	62	6.27	0.40	1.20
	Powder	—	511	0.24[c]	—	56	3.36[d]	0.71	2.26
NPhBPy-HC	Cyclohexane	435 (3.77), 463 (2.67)]	493, 515	0.45[b]	1.31	54	3.57	1.26	1.54
	Powder	—	540	0.32[c]	—	40	1.28[d]	2.50	5.31
NFBPy-HC	Cyclohexane	444 (4.19), 470 (3.72)	493, 522	0.49[b]	0.99	48	2.48	1.98	2.05
	Powder	—	571	0.60[c]	—	62	2.78[d]	2.16	1.43
BiNFBPy-HC	Cyclohexane	451 (8.09), 468 (8.84)	496, 525	0.41[b]	1.21	28	2.31	1.77	2.55
	Powder	—	571	0.41[c]	—	66	1.94[d]	2.11	3.04
BiNPy-HC	Cyclohexane	362 (2.85)	436, 458	0.40[b]	4.69	39	9.82	0.41	0.61

[a] Only the maxima of the longest wavelength band are shown. [b] Calculated using coumarin 307 as a standard. [c] Absolute quantum yields determined using an integrating sphere. [d] Average lifetime calculated using the equation $A_i\tau_i/\Sigma A_i\tau_i$, where A_i is the preexponential for lifetime τ_i.

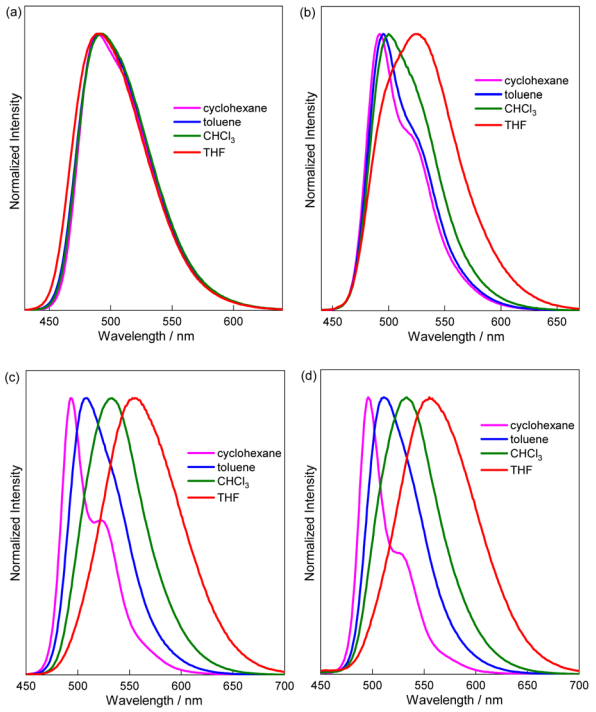

Fig. 4 Fluorescence spectra ($c = 1.0 \times 10^{-5}$ M and $\lambda_{ex} = 400$ nm) of (a) PhBPy-HC, (b) NPhBPy-HC, (c) NFBPy-HC, and (d) BiNFBPy-HC in various solvents.

the fluorescence solvatochromism, another notable thing is that the bis-fused derivative **BiNFBPy-HC** exhibits fluorescence spectra that are very close to those of **NFBPy-HC**, albeit with slightly lower Φ_F values. These fluorescence solvatochromism results suggest the first excited (S_1) state of **PhBPy-HC** lacks significant CT character, while **NPhBPy-HC** displays partial CT nature due to the presence of the electron donating $Ph_2NC_6H_4$ group. The CT character becomes even more pronounced in **NFBPy-HC** and **BiNFBPy-HC** as a result of the replacement of Ph with C_6F_5 at the boron center. These results hence confirm that the fusion of the B ← N Lewis pair helps enhance the electron affinity and tuning the substituent on the boron atom allows further modulation of this electron-accepting ability.

Theoretical calculations

To gain deeper insight into structure–property relationships, we conducted density functional theory (DFT) and time-dependent DFT (TD-DFT) calculations at the B3LYP-D3(BJ)/6-31g(d) level. For all B ← N Lewis pair-fused [6]helicenes, the longest wavelength absorption band can be assigned to the $S_0 \rightarrow S_1$ excitation process through comparison between the experimental and simulated absorption spectra (Fig. 5 and S10). For the three mono-fused [6]helicene derivatives, this excitation is predominantly composed of the HOMO → LUMO transition. Both the HOMO and the LUMO of **PhBPy-HC** are distributed over the pyridyl ring and the four adjacent benzene rings of the [6]helicene skeleton. Hence, the $S_0 \rightarrow S_1$ excitation of **PhBPy-HC** is characterized by a π–π^* transition process. Upon introduction of a $Ph_2NC_6H_4$ group into **NPhBPy-HC**, the HOMO becomes further delocalized over the entire $Ph_2NC_6H_4$ group while the LUMO remains almost unchanged. As a result, the introduction of triphenylamine imparts the $S_0 \rightarrow S_1$ transition with a partial intramolecular CT feature. Moreover, the introduction of $Ph_2NC_6H_4$ raises both HOMO and LUMO energy levels with a more pronounced increase for the HOMO ($\Delta E = 0.26$ eV) than for the LUMO ($\Delta E = 0.06$ eV). Although the aryl group on boron does not contribute to the frontier orbitals due to its tetracoordinated structure, the change of the aryl substituent on boron from phenyl in **NPhBPy-HC** to the more electron-withdrawing C_6F_5 in **NFBPy-HC** lowers both HOMO ($\Delta E = 0.15$ eV) and LUMO ($\Delta E = 0.24$ eV) energy levels with the LUMO decreased more greatly. Notably, the contribution of the [6]helicene core to the HOMO becomes less significant in **NFBPy-HC**, suggesting a stronger intramolecular CT character for $S_0 \rightarrow S_1$ excitation of **NFBPy-HC**. Thus, **NPhBPy-HC** and **NFBPy-HC** can be regarded as D–A systems. Consistent with these electronic changes, the calculated absorption wavelength for $S_0 \rightarrow S_1$ excitation gradually red shifts from **PhBPy-HC** to **NPhBPy-HC** and **NFBPy-HC** together with the progressive increase in the oscillator strength.

From mono-fused **NFBPy-HC** to bis-fused **BiNFBPy-HC**, the HOMO and LUMO energy levels remain nearly unchanged. However, the electronic distributions of the HOMO and LUMO change markedly with the fusion of additional B ← N Lewis pairs. In **BiNFBPy-HC**, the HOMO and LUMO are degenerate to HOMO−1 and LUMO+1, respectively. The HOMO is mainly distributed over two $Ph_2NC_6H_4$ units and the central [6]helicene, while the HOMO−1 excludes the contribution from [6]helicene. In contrast, the LUMO and LUMO+1 are mainly localized on [6]helicene and two pyridyl rings. It was noted that HOMO−1 and LUMO+1 are C_2-antisymmetric while the HOMO and LUMO are C_2-symmetric. The $S_0 \rightarrow S_1$ excitation of **BiNFBPy-HC**, which is dominated by HOMO → LUMO+1 (66%) and HOMO−1 → LUMO (19%) transitions, is symmetry permitted and exhibits much larger oscillator strength than **NFBPy-HC**. These results suggest the efficient exciton coupling between two fused moieties through the central [6]helicene skeleton in **BiNFBPy-HC** and this compound can be categorized as a quadrupolar D–A–D system. While the accuracy of calculated excitation energies is not sufficiently high at this computation level, these calculated results clearly demonstrate the CT feature of the $S_0 \rightarrow S_1$ transition for three derivatives containing electron-donating $Ph_2NC_6H_4$, which agrees well with their fluorescence solvatochromism. Furthermore, the simulated absorption spectra successfully reproduced the gradual red shift of absorption and increase of absorption intensity with increasing CT character from **PhBPy-HC** to **NPhBPy-HC** and **NFBPy-HC**, as well as the remarkable increase of absorption intensity from **NFBPy-HC** to **BiNFBPy-HC** as a result of effective exciton coupling.[67]

Fluorescence properties in the solid state

The high emission efficiency in the solid state is also a critical property for CPL emitters. Herein, the solid-state fluorescence properties of these B ← N Lewis pair-fused [6]helicenes were

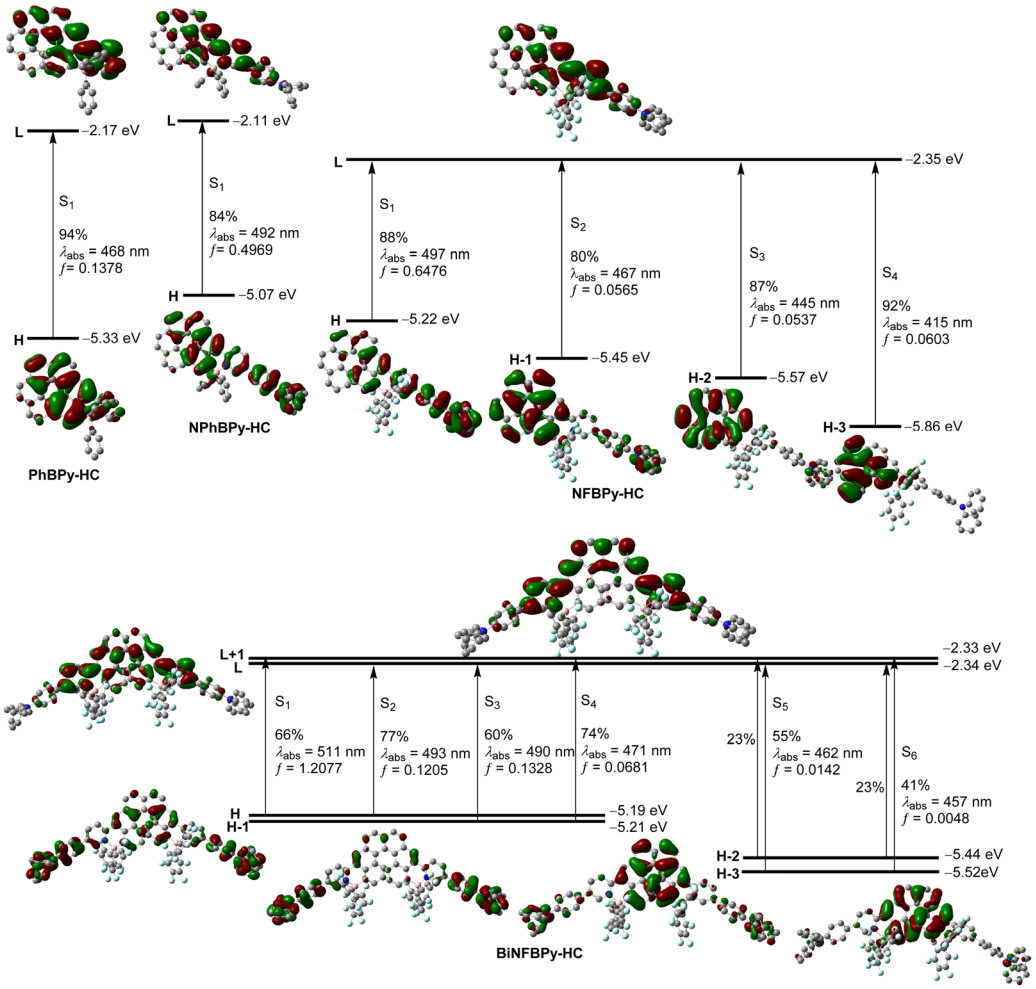

Fig. 5 Kohn–Sham energy levels, pictorial drawing of frontier orbitals, and transitions of B ← N Lewis pair-fused [6]helicenes at the S_0 geometries, calculated at the TD-B3LYP-D3(BJ)/6-31g(d) level.

also investigated (Fig. 6, Table 1). For all the compounds, the fluorescence of powders appears at longer wavelengths even compared with their emission in THF solution, with red shifts within the range of 14–20 nm. The bathochromic shift indicates the presence of intermolecular π–π interactions. Notably, no significant fluorescence quenching was observed when going from cyclohexane to the powder form despite the presence of intermolecular π–π interactions in the solid state. From cyclohexane to the powder form, only **NPhBPy-HC** exhibits slight fluorescence quenching among the four B ← N Lewis pair-fused [6]helicenes. In contrast, the Φ_F values of **PhBPy-HC** and **BiNFBPy-HC** remain nearly unchanged. Remarkably, the Φ_F of **NFBPy-HC** in the powder form is even much higher than in cyclohexane, reaching a very high value of 0.60. Consequently, all these B ← N Lewis pair-fused [6]helicenes exhibit bright fluorescence in the solid state with moderate to high efficiency ($\Phi_F = 0.24$–0.60). Moreover, the emission colours can be facilely tuned from green (**PhBPy-HC**, $\lambda_{em} = 511$ nm) to yellow (**NPhBPy-HC**, $\lambda_{em} = 540$ nm) and then to orange (**NFBPy-HC** and **BiNFBPy-HC**, $\lambda_{em} = 571$ nm), highlighting the great utility of B ← N Lewis pair fusion with helicenes for achieving efficient and tunable solid-state emission.

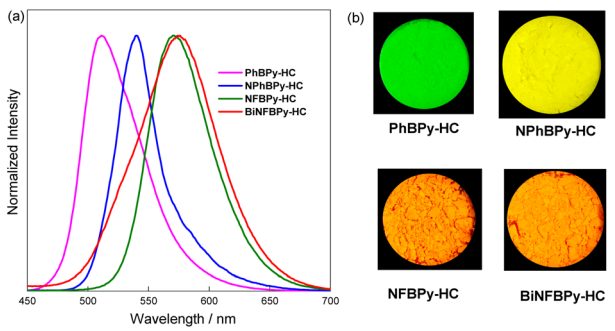

Fig. 6 (a) Fluorescence spectra ($\lambda_{ex} = 400$ nm) and (b) photographs under UV irradiation at 365 nm for the powder of B ← N Lewis pair-fused [6]helicenes.

Two-photon absorption properties

Considering the electron affinity endowed by B ← N Lewis pair fusion, we then investigated the TPA properties of these B ← N Lewis pair-fused [6]helicene compounds. The TPA spectra were

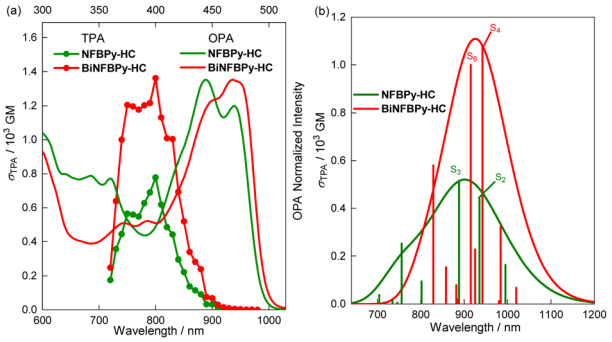

Fig. 7 (a) Rescaled one-photon absorption spectra and two-photon absorption spectra of B ← N Lewis pair-fused [6]helicenes in THF. (b) Calculated TPA spectra from the S_0 state to various excited states at the optimized S_0 geometries of **NFBPy-HC** and **BiNFBPy-HC**, calculated at TD-B3LYP-D3(BJ)/6-31G(d).

measured in THF *via* a two-photon-excited fluorescence (TPEF) method using coumarin 485 as the standard compound with femtosecond laser excitation at wavelengths of 720–1000 nm (Fig. 7a). Unfortunately, **PhBPy-HC** decomposed during the measurement, as indicated by the complete disappearance of fluorescence. Interestingly, the other three compounds exhibit very strong TPA absorption. The highest δ_{TPA} values were determined to be 604 GM at 790 nm for **NPhBPy-HC**, 777 GM at 800 nm for **NFBPy-HC**, 1361 GM at 800 nm for **BiNFBPy-HC**, respectively. In addition, these three compounds can retain intense TPA absorption over a relatively broad region: 560–604 GM within 750–800 nm for **NPhBPy-HC**, 564–777 GM within 750−810 nm for **NFBPy-HC** and 1177–1360 GM within 750−800 nm for **BiNFBPy-HC**. Notably, the δ_{TPA} maximum of **BiNFBPy-HC** is nearly 1.8 times greater than that of **NPhBPy-HC** and **NFBPy-HC** and is among the largest values reported for the helicene derivatives.[15,16,68,69]

The comparison between the TPA and the rescaled one-photon absorption (OPA) spectra revealed that the intense TPA bands of these three compounds correspond to dark transitions in the OPA and arise from excitations to a higher excited state. The theoretical calculations of TPA properties further supported this point (Fig. 7b, S11 and Table S7). The intense TPA band of **BiNFBPy-HC** primarily consists of $S_0 \rightarrow S_4$ and $S_0 \rightarrow S_6$ transitions with the $S_0 \rightarrow S_4$ transition giving the highest theoretical δ_{TPA}. The $S_0 \rightarrow S_4$ transition of **BiNFBPy-HC** is dominated by the HOMO−1 → LUMO+1 transition (74%), while the composition of $S_0 \rightarrow S_6$ is more complex. The first two important components are HOMO−3 → LUMO+1 (41%) and HOMO−2 → LUMO (23%) transitions. Both HOMO−2 and HOMO−3 are distributed over the central [6]helicene core with HOMO−2 spreading to two Ph_2N groups. It was noted that HOMO−1 → LUMO+1, HOMO−3 → LUMO+1, and HOMO−2 → LUMO transitions are symmetry prohibited, which is consistent with the low oscillator strengths of the corresponding OPA transitions ($f = 0.0681$ for of $S_0 \rightarrow S_4$; 0.0048 for $S_0 \rightarrow S_6$). For the mono-fused **NPhBPy-HC** and **NFBPy-HC**, which differ in the substituent at the boron center, the theoretical δ_{TPA} maxima originate from $S_0 \rightarrow S_2$ and $S_0 \rightarrow S_3$ excitations, respectively. Both transitions greatly contribute to TPA. In addition, the intense TPA band of **NPhBPy-HC** also involves the $S_0 \rightarrow S_4$ excitation process. The $S_0 \rightarrow S_2$, $S_0 \rightarrow S_3$ and $S_0 \rightarrow S_4$ excitations correspond to the transitions from HOMO−1, HOMO−2 and HOMO−3 to LUMO, respectively, for both compounds. Moreover, these two compounds show similar electronic distributions for HOMO−1, HOMO−2 and HOMO−3 orbitals. From HOMO−1 to HOMO−3, the electronic distribution gradually becomes more delocalized. The HOMO−1 is delocalized over the [6]helicene core skeleton and $Ph_2NC_6H_4$ group, while HOMO−2 is only localized on the [6]helicene unit and HOMO−3 is located on a portion of the [6]helicene moiety. The theoretical calculations of TPA properties clearly indicate the significance of B ← N Lewis pair fusion for the promising TPA of the three amino-containing B ← N Lewis pair-fused [6]helicenes and the much more enhanced δ_{TPA} of bis-fused **BiNFBPy-HC** than the mono-fused **NPhBPy-HC** and **NFBPy-HC**. The highly symmetric charge transfer together with the extended π-conjugation in **BiNFBPy-HC** remarkably increases the probability of TPA transitions, thus leading to a much larger δ_{TPA}.[18]

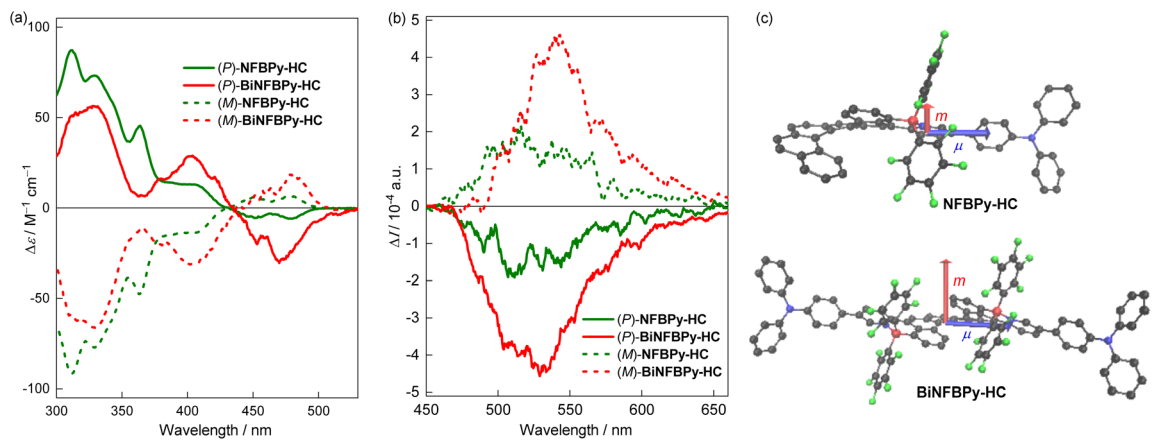

Fig. 8 (a) CD ($c = 2.0 \times 10^{-5}$ M) and (b) CPL ($c = 2.0 \times 10^{-5}$ M, $\lambda_{ex} = 370$ nm) spectra of **NFBPy-HC** and **BiNFBPy-HC** in cyclohexane. (c) $S_0 \rightarrow S_1$ transition electronic (blue) and magnetic (red) dipole moments of **NFBPy-HC** and **BiNFBPy-HC**, calculated by TD-DFT at the B3LYP-D3(BJ)/6-31g(d) level for *M*-enantiomers.

Table 2 Chiroptical properties of NFBPy-HC and BiNFBPy-HC

	CD[a]		CPL[a]		$S_0 \rightarrow S_1$ transition[b]					$S_1 \rightarrow S_0$ transition[b]			
	$\lvert g_{abs}\rvert/10^{-4}$		$\lvert g_{lum}\rvert/10^{-4}$	B_{CPL}/M^{-1} cm^{-1}	$\lvert\mu\rvert/10^{-17}$ esu cm	$\lvert m\rvert/10^{-20}$ erg G^{-1}	θ/°	$\lvert g_{abs}\rvert^{cal}/10^{-4}$		$\lvert\mu\rvert/10^{-17}$ esu cm	$\lvert m\rvert/10^{-20}$ erg G^{-1}	θ/°	$\lvert g_{lum}\rvert^{cal}/10^{-4}$
NFBPy-HC	2.17 (480)		3.31 (515)	3.0	0.83	1.91	87.0	4.85		0.83	1.83	87.0	4.71
BiNFBPy-HC	5.00 (483)		7.37 (543)	13.2	1.15	4.85	87.0	9.04		1.08	4.45	86.7	9.32

[a] Measured in cyclohexane solution. [b] Calculated by TD-DTF at the B3LYP-D3(BJ)/6-31g(d) level for *M*-enantiomers.

Chiroptical properties

Finally, we proceeded to prepare their enantiomerically pure forms to investigate their chiroptical properties. Due to the extremely poor solubility of **PhBPy-HC** and **NPhBPy-HC**, no appropriate conditions for chiral resolution could be established. The enantiomeric pairs of **NFBPy-HC** and **BiNFBPy-HC** were successfully obtained through high-performance liquid chromatography (HPLC) with a chiral column (Fig. S7–S8 and Tables S2–S3). The experimental CD and CPL spectra in cyclohexane are shown in Fig. 8 with the corresponding data summarized in Table 2. The absolute configurations were assigned through the comparison between the experimental and theoretically simulated ECD spectra (Fig. S11b), which show the same signs for the longest and shortest wavelength bands above 300 nm. For both compounds, the (*P*)-isomer corresponds to the first eluted fraction.

In cyclohexane, nearly perfect mirror images were observed for the CD and CPL spectra of (*P*)- and (*M*)-isomers. The (*P*)-isomers of **NFBPy-HC** and **BiNFBPy-HC** display the longest wavelength CD bands at around 480 nm with a negative sign, while the strongest CD bands were observed at approximately 330 nm with a positive sign. The longest wavelength CD bands are assignable to the $S_0 \rightarrow S_1$ transition and the corresponding CD dissymmetry factors (g_{abs}, defined as $\Delta\varepsilon/\varepsilon$) are determined to be -2.17×10^{-4} and -5.00×10^{-4} for (*P*)-**NFBPy-HC** and (*P*)-**BiNFBPy-HC**, respectively. The change of solvent from cyclohexane to THF caused negligible variations in the CD spectra, in terms of either position or intensity (Fig. S9). Remarkably, these two compounds display clearly mirror-imaged CPL signals in both nonpolar cyclohexane and polar THF, with the signs consistent with the corresponding longest CD bands. In cyclohexane, the $|g_{lum}|$ values are up to 3.31×10^{-4} for **NFBPy-HC** and 7.37×10^{-4} for **BiNFBPy-HC**, respectively. Upon changing the solvent from cyclohexane to THF, the CPL spectra of both compounds are red-shifted by about 70 nm, which is consistent with their fluorescence solvatochromism. Notably, the bis-fused **BiNFBPy-HC** has significantly higher $|g_{abs}|$ for the longest wavelength band as well as larger $|g_{lum}|$ compared to the mono-fused **NFBPy-HC**. Unfortunately, the CPL signals are nearly undetectable in both film and powder forms, although strong fluorescence emission is retained in the solid state.

To gain further insight into the chiroptical properties of the S_1 state, the theoretical $|g_{abs}|$ and $|g_{lum}|$ values for the $S_0 \rightarrow S_1$ and $S_1 \rightarrow S_0$ transitions were herein analysed (Table 2 and Fig. 8c and S13). Theoretically, the dissymmetry factors can be predicted using $4|\mu||m|\cos\theta/(|\mu|^2 + |m|^2)$, where μ and m are the electronic and magnetic transition dipole moments, respectively, and θ is the angle between them. Because μ of organic molecules is hundreds of times larger than m, this expression can be simplified as $4|m|\cos\theta/|\mu|$.[70,71] For each compound, all the calculated parameters of $S_0 \rightarrow S_1$ excitation are comparable to those of $S_1 \rightarrow S_0$ deactivation. Notably, these two compounds show almost the same θ and close $|\mu|$, whereas the $|m|$ of **BiNFBPy-HC** is about 2.5 times that of **NFBPy-HC**. Consequently, the calculated $|g_{abs}|$ and $|g_{lum}|$ values of **BiNFBPy-HC** are nearly two times those of **NFBPy-HC**, which is consistent with the

experimental trend. These results suggest the structural evolution from a dipolar to a quadrupolar architecture helps enhance $|m|$ and thereby increase transition dissymmetry factors. Another notable thing is that m is nearly perpendicular to μ for both compounds ($\theta \approx 87°$), giving a very small $\cos\theta$. It should be the small $\cos\theta$ that results in unideal $|g_{abs}|$ and $|g_{lum}|$ values. Although $|g_{lum}|$ of **BiNFBPy-HC** is not quite high, its B_{CPL} of **BiNFBPy-HC** can reach 13.2 M^{-1} cm^{-1} in cyclohexane, an excellent value among B ← N Lewis pair-functioned helicenes, due to its very high ε and good Φ_F.[58,59] Moreover, the B_{CPL} of **BiNFBPy-HC** is more than four times that of **NFBPy-HC** (3.0 M^{-1} cm^{-1}), highlighting the superior chiroptical properties of bis-fused quadrupolar **BiNFBPy-HC** over mono-fused dipolar **NFBPy-HC**.

Conclusions

In summary, we have successfully synthesized a new family of [6]helicene derivatives, which are fused with six-membered B ← N heterocycles, *via* N-directed electrophilic borylation of 2-pyridyl-substituted [6]helicene precursors. Their photophysical properties were comprehensively investigated both experimentally and theoretically to elucidate the effect of structural modification. It was revealed that ε and Φ_F increase progressively from parent [6]helicene to **PhBPy-HC** by fusion with the B ← N Lewis pair and are further enhanced in **NPhBPy-HC** due to the introduction of the electron-donor *p*-$Ph_2NC_6H_4$ into pyridyl and thus the intramolecular CT nature. ε and Φ_F of the mono-fused compounds reach maxima in **NFBPy-HC**, which displays more pronounced intramolecular CT characteristics as a result of the displacement of Ph on the boron atom with a stronger electron-withdrawing C_6F_5 group. The ε and Φ_F **NFBPy-HC** are as high as 3.70 × 10^4 M^{-1} cm^{-1} and 0.49, respectively. From mono-fused dipolar **NFBPy-HC** to bis-fused quadrupolar **BiNFBPy-HC**, although Φ_F slightly decreases to 0.41, ε more than doubles to 8.84 × 10^4. Notably, all three B ← N fused [6]helicenes, **NPhBPy-HC**, **NFBPy-HC**, and **BiNFBPy-HC**, which contain electron donating *p*-$Ph_2NC_6H_4$, exhibit excellent TPA properties with δ_{TPA} maxima in the range of 604∼1361 GM. In particular, the bis-fused quadrupolar **BiNFBPy-HC** displays significantly improved TPA properties compared to mono-fused dipolar analogues due to the efficient electron coupling among its branches. Moreover, the enantiomerically pure forms of **NFBPy-HC** and **BiNFBPy-HC** emit notable CPL signals. Again, **BiNFBPy-HC** has significantly higher $|g_{abs}|$ for the longest wavelength band and larger $|g_{lum}|$ compared to **NFBPy-HC**, which is ascribed to enhancement of magnetic transition dipoles. Hence, the structural evolution from a dipole to a quadrupole can simultaneously enhance absorptivity, TPA cross section and CPL dissymmetry. Owing to the large ε, good Φ_F and moderate $|g_{lum}|$, the bis-fused quadrupolar **BiNFBPy-HC** achieves a remarkably high B_{CPL} (13.2 M^{-1} cm^{-1}), representing a very rare example of organic molecules that integrate excellent CPL and TPA properties. Regarding the photophysical properties, another notable thing is that all these B ← N fused [6]helicenes display intense fluorescence in the solid state (Φ_F = 0.24–0.60 in powder form) with tunable emission colours from green to yellow and then to orange. Considering the facile preparation, great CPL performance, outstanding TPA properties, and efficient solid-state emission of **BiNFBPy-HC**, it is expected to be an excellent emitter. Furthermore, we believe that the valuable results about the structure–property relationships will lay a solid foundation for the rational design of new CPL-active molecules, especially those with integrated great CPL and TPA properties.

Author contributions

C.-H. Zhao conceived the project. M. Wang synthesized the compounds and conducted all characterization and theoretical studies under the supervision of C.-H. Zhao and Z.-Q. Liu. C.-H. Zhao analyzed the data and wrote the manuscript. All authors commented on it.

Conflicts of interest

There are no conflicts to declare.

Data availability

2488475 (**PhBPy-HC**) and 2488477 (**NFBPy-HC**) contain the supplementary crystallographic data for this paper.[72a,b]

Supplementary information (SI): preparation, photophysical properties, calculation details, and NMR spectra. See DOI: https://doi.org/10.1039/d5sc08697c.

Acknowledgements

We gratefully acknowledge financial support from the Natural Science Foundation of Shandong Province (Grant No. ZR2024MB033) and the National Natural Science Foundation of China (Grant No. 21971150 and U2330106). The HPC Cloud Platform of Shandong University is also sincerely acknowledged for its support of the theoretical calculations.

Notes and references

1 Y. Yang, R. C. da Costa, D. M. Smilgies, A. J. Campbell and M. J. Fuchter, Induction of Circularly Polarized Electroluminescence from an Achiral Light-Emitting Polymer *via* a Chiral Small-Molecule Dopant, *Adv. Mater.*, 2013, **25**, 2624–2628.

2 F. Furlan, J. M. Moreno-Naranjo, N. Gasparini, S. Feldmann, J. Wade and M. J. Fuchter, Chiral materials and mechanisms for circularly polarized light-emitting diodes, *Nat. Photonics*, 2024, **18**, 658–668.

3 Y. Yang, R. C. da Costa, M. J. Fuchter and A. J. Campbell, Circularly polarized light detection by a chiral organic semiconductor transistor, *Nat. Photonics*, 2013, **7**, 634–638.

4 Y. Chen, J. Gao and X. Yang, Chiral Grayscale Imaging with Plasmonic Metasurfaces of Stepped Nanoapertures, *Adv. Optical Mater.*, 2019, **7**, 1801467.

5 R. Hassey, E. J. Swain, N. I. Hammer, D. Venkataraman and M. D. Barnes, Probing the chiroptical response of a single molecule, *Science*, 2006, **314**, 1437–1439.
6 P. Stachelek, S. Serrano-Buitrago, B. L. Maroto, R. Pal and S. de la Moya, Circularly Polarized Luminescence Bioimaging Using Chiral BODIPYs: A Model Scaffold for Advancing Unprecedented CPL Microscopy Using Small Full-Organic Probes, *ACS Appl. Mater. Interfaces*, 2024, **16**, 67246–67254.
7 E. M. Sánchez-Carnerero, A. R. Agarrabeitia, F. Moreno, B. L. Maroto, G. Muller, M. J. Ortiz and S. de la Moya, Circularly Polarized Luminescence from Simple Organic Molecules, *Chem.–Eur. J.*, 2015, **21**, 13488–13500.
8 G. Longhi, E. Castiglioni, J. Koshoubu, G. Mazzeo and S. Abbate, Circularly Polarized Luminescence: A Review of Experimental and Theoretical Aspects, *Chirality*, 2016, **28**, 696–707.
9 L. Arrico, L. Di Bari and F. Zinna, Quantifying the Overall Efficiency of Circularly Polarized Emitters, *Chem.–Eur. J.*, 2021, **27**, 2920–2934.
10 F. Terenziani, C. Katan, E. Badaeva, S. Tretiak and M. Blanchard-Desce, Enhanced Two-Photon Absorption of Organic Chromophores: Theoretical and Experimental Assessments, *Adv. Mater.*, 2008, **20**, 4641–4678.
11 M. Pawlicki, H. A. Collins, R. G. Denning and H. L. Anderson, Two-Photon Absorption and the Design of Two-Photon Dyes, *Angew. Chem., Int. Ed.*, 2009, **48**, 3244–3266.
12 H. M. Kim and B. R. Cho, Small-Molecule Two-Photon Probes for Bioimaging Applications, *Chem. Rev.*, 2015, **115**, 5014–5055.
13 P. Stachelek, L. MacKenzie, D. Parker and R. Pal, Circularly polarised luminescence laser scanning confocal microscopy to study live cell chiral molecular interactions, *Nat. Commun.*, 2022, **13**, 553.
14 B. Fabri, D. F. De Rosa, D. J. Black, R. Mucci, A. Krimovs, R. Pal and J. Lacour, Two-photon Excitation of Bright Diaza[4]Helicenes for Isotropic and Circularly Polarized Emission, *Chem.–Eur. J.*, 2025, **31**, e202501212.
15 C. M. Cruz, S. Castro-Fernández, E. Maçôas, J. M. Cuerva and A. G. Campaña, Undecabenzo[7]superhelicene: A Helical Nanographene Ribbon as a Circularly Polarized Luminescence Emitter, *Angew. Chem., Int. Ed.*, 2018, **57**, 14782–14786.
16 C. M. Cruz, I. R. Márquez, I. F. A. Mariz, V. Blanco, C. Sánchez-Sánchez, J. M. Sobrado, J. A. Martín-Gago, J. M. Cuerva, E. Maçôas and A. G. Campaña, Enantiopure distorted ribbon-shaped nanographene combining two-photon absorption-based upconversion and circularly polarized luminescence, *Chem. Sci.*, 2018, **9**, 3917–3924.
17 P. Reine, A. M. Ortuño, I. F. A. Mariz, M. Ribagorda, J. M. Cuerva, A. G. Campaña, E. Maçôas and D. Miguel, Simple Perylene Diimide Cyclohexane Derivative With Combined CPL and TPA Properties, *Front. Chem.*, 2020, **8**, 306.
18 M. Albota, D. Beljonne, J.-L. Bredas, J. E. Ehrlich, J.-Y. Fu, A. A. Heikal, S. E. Hess, T. Kogej, M. D. Levin and S. R. Marder, Design of organic molecules with large two-photon absorption cross sections, *Science*, 1998, **281**, 1653–1656.
19 B. Jagatap and W. J. Meath, Contributions of permanent dipole moments to molecular multiphoton excitation cross sections, *J. Opt. Soc. Am. B*, 2002, **19**, 2673–2681.
20 T.-C. Lin, G. S. He, P. N. Prasad and L.-S. Tan, Degenerate nonlinear absorption and optical power limiting properties of asymmetrically substituted stilbenoid chromophores, *J. Mater. Chem.*, 2004, **14**, 982–991.
21 L. Beverina, J. Fu, A. Leclercq, E. Zojer, P. Pacher, S. Barlow, E. W. Van Stryland, D. J. Hagan, J.-L. Brédas and S. R. Marder, Two-photon absorption at telecommunications wavelengths in a dipolar chromophore with a pyrrole auxiliary donor and thiazole auxiliary acceptor, *J. Am. Chem. Soc.*, 2005, **127**, 7282–7283.
22 C.-L. Sun, Q. Liao, T. Li, J. Li, J.-Q. Jiang, Z.-Z. Xu, X.-D. Wang, R. Shen, D.-C. Bai, Q. Wang, S.-X. Zhang, H.-B. Fu and H.-L. Zhang, Rational design of small indolic squaraine dyes with large two-photon absorption cross section, *Chem. Sci.*, 2015, **6**, 761–769.
23 M. Rumi, J. E. Ehrlich, A. A. Heikal, J. W. Perry, S. Barlow, Z. Hu, D. McCord-Maughon, T. C. Parker, H. Röckel and S. Thayumanavan, Structure−property relationships for two-photon absorbing chromophores: bis-donor diphenylpolyene and bis (styryl) benzene derivatives, *J. Am. Chem. Soc.*, 2000, **122**, 9500–9510.
24 O. Mongin, L. Porrès, M. Charlot, C. Katan and M. Blanchard-Desce, Synthesis, Fluorescence, and Two-Photon Absorption of a Series of Elongated Rodlike and Banana-Shaped Quadrupolar Fluorophores: A Comprehensive Study of Structure–Property Relationships, *Chem.–Eur. J.*, 2007, **13**, 1481–1498.
25 Y. Jiang, Y. Wang, J. Hua, J. Tang, B. Li, S. Qian and H. Tian, Multibranched triarylamine end-capped triazines with aggregation-induced emission and large two-photon absorption cross-sections, *Chem. Commun.*, 2010, **46**, 4689–4691.
26 J. Shao, Z. Guan, Y. Yan, C. Jiao, Q.-H. Xu and C. Chi, Synthesis and Characterizations of Star-Shaped Octupolar Triazatruxenes-Based Two-Photon Absorption Chromophores, *J. Org. Chem.*, 2011, **76**, 780–790.
27 Y. M. Poronik, V. Hugues, M. Blanchard-Desce and D. T. Gryko, Octupolar Merocyanine Dyes: A New Class of Nonlinear Optical Chromophores, *Chem.–Eur. J.*, 2012, **18**, 9258–9266.
28 T. Mori, Chiroptical Properties of Symmetric Double, Triple, and Multiple Helicenes, *Chem. Rev.*, 2021, **121**, 2373–2412.
29 W.-L. Zhao, M. Li, H.-Y. Lu and C.-F. Chen, Advances in helicene derivatives with circularly polarized luminescence, *Chem. Commun.*, 2019, **55**, 13793–13803.
30 M. Cei, L. Di Bari and F. Zinna, Circularly polarized luminescence of helicenes: A data-informed insight, *Chirality*, 2023, **35**, 192–210.
31 M. Sapir and E. Vander Donckt, Intersystem crossing in the helicenes, *Chem. Phys. Lett.*, 1975, **36**, 108–110.

32 J. Birks, D. Birch, E. Cordemans and E. Vander Donckt, Fluorescence of the higher helicenes, *Chem. Phys. Lett.*, 1976, **43**, 33–36.
33 H. Oyama, K. Nakano, T. Harada, R. Kuroda, M. Naito, K. Nobusawa and K. Nozaki, Synthetic Route to Highly Luminescent sila[7]helicene, *Org. Lett.*, 2013, **15**, 2104–2107.
34 T. Katayama, S. Nakatsuka, H. Hirai, N. Yasuda, J. Kumar, T. Kawai and T. Hatakeyama, Two-Step Synthesis of Boron-Fused Double Helicenes, *J. Am. Chem. Soc.*, 2016, **138**, 5210–5213.
35 K. Dhbaibi, L. Favereau and J. Crassous, Enantioenriched Helicenes and Helicenoids Containing Main-Group Elements (B, Si, N, P), *Chem. Rev.*, 2019, **119**, 8846–8953.
36 J.-K. Li, X.-Y. Chen, Y.-L. Guo, X.-C. Wang, A. C. H. Sue, X.-Y. Cao and X.-Y. Wang, B,N-Embedded Double Hetero[7] helicenes with Strong Chiroptical Responses in the Visible Light Region, *J. Am. Chem. Soc.*, 2021, **143**, 17958–17963.
37 F. Zhang, F. Rauch, A. Swain, T. B. Marder and P. Ravat, Efficient Narrowband Circularly Polarized Light Emitters Based on 1,4-B,N-embedded Rigid Donor–Acceptor Helicenes, *Angew. Chem., Int. Ed.*, 2023, **62**, e202218965.
38 A. Nowak-Król, P. T. Geppert and K. R. Naveen, Boron-containing helicenes as new generation of chiral materials: opportunities and challenges of leaving the flatland, *Chem. Sci.*, 2024, **15**, 7408–7440.
39 F. Zhang, V. Brancaccio, F. Saal, U. Deori, K. Radacki, H. Braunschweig, P. Rajamalli and P. Ravat, Ultra-Narrowband Circularly Polarized Luminescence from Multiple 1,4-Azaborine-Embedded Helical Nanographenes, *J. Am. Chem. Soc.*, 2024, **146**, 29782–29791.
40 T. Hatakeyama, S. Hashimoto, T. Oba and M. Nakamura, Azaboradibenzo[6]helicene: Carrier Inversion Induced by Helical Homochirality, *J. Am. Chem. Soc.*, 2012, **134**, 19600–19603.
41 Y. Appiarius, S. Míguez-Lago, P. Puylaert, N. Wolf, S. Kumar, M. Molkenthin, D. Miguel, T. Neudecker, M. Juríček, A. G. Campaña and A. Staubitz, Boosting quantum yields and circularly polarized luminescence of penta- and hexahelicenes by doping with two BN-groups, *Chem. Sci.*, 2024, **15**, 466–476.
42 Y. Jiao, Z. Sun, Z. Wang, Y. Fu and F. Zhang, Synthesis of Nonsymmetric NBN-Embedded [6]- and [7]Helicenes with Amplified Activities, *Org. Lett.*, 2023, **25**, 8766–8770.
43 T. Fujikawa, Y. Segawa and K. Itami, Synthesis, Structures, and Properties of π-Extended Double Helicene: A Combination of Planar and Nonplanar π-Systems, *J. Am. Chem. Soc.*, 2015, **137**, 7763–7768.
44 D. Reger, P. Haines, F. W. Heinemann, D. M. Guldi and N. Jux, Oxa[7]superhelicene: A π-Extended Helical Chromophore Based on Hexa-peri-hexabenzocoronenes, *Angew. Chem., Int. Ed.*, 2018, **57**, 5938–5942.
45 F. Saal, F. Zhang, M. Holzapfel, M. Stolte, E. Michail, M. Moos, A. Schmiedel, A.-M. Krause, C. Lambert, F. Würthner and P. Ravat, [*n*]Helicene Diimides (n = 5, 6, and 7): Through-Bond *versus* Through-Space Conjugation, *J. Am. Chem. Soc.*, 2020, **142**, 21298–21303.
46 Z. Qiu, C.-W. Ju, L. Frédéric, Y. Hu, D. Schollmeyer, G. Pieters, K. Müllen and A. Narita, Amplification of Dissymmetry Factors in π-Extended [7]- and [9]Helicenes, *J. Am. Chem. Soc.*, 2021, **143**, 4661–4667.
47 R. K. Dubey, M. Melle-Franco and A. Mateo-Alonso, Inducing Single-Handed Helicity in a Twisted Molecular Nanoribbon, *J. Am. Chem. Soc.*, 2022, **144**, 2765–2774.
48 F. Zhao, J. Zhao, H. Liu, Y. Wang, J. Duan, C. Li, J. Di, N. Zhang, X. Zheng and P. Chen, Synthesis of π-Conjugated Chiral Organoborane Macrocycles with Blue to Near-Infrared Emissions and the Diradical Character of Cations, *J. Am. Chem. Soc.*, 2023, **145**, 10092–10103.
49 X. Tian, K. Shoyama, B. Mahlmeister, F. Brust, M. Stolte and F. Würthner, Naphthalimide-Annulated [n]Helicenes: Red Circularly Polarized Light Emitters, *J. Am. Chem. Soc.*, 2023, **145**, 9886–9894.
50 M. Wang, M.-Y. Zhang and C.-H. Zhao, Brightening Up Circularly Polarized Luminescence of [6]Helicenes by Fusion with BN-Heterocycles, *Org. Lett.*, 2025, **27**, 1823–1828.
51 A. C. Shaikh, D. S. Ranade, S. Thorat, A. Maity, P. P. Kulkarni, R. G. Gonnade, P. Munshi and N. T. Patil, Highly emissive organic solids with remarkably broad color tunability based on N,C-chelate, four-coordinate organoborons, *Chem. Commun.*, 2015, **51**, 16115–16118.
52 C. Zhu and L. Fang, Locking the Coplanar Conformation of π-Conjugated Molecules and Macromolecules Using Dynamic Noncovalent Bonds, *Macromol. Rapid Commun.*, 2018, **39**, 1700241.
53 A. Sahoo, A. Patel, R. A. Lalancette and F. Jäkle, B ← N Lewis Pair Fusion of N,N-Diaryldihydrophenazines: Effect on Structural, Electronic, and Emissive Properties, *Angew. Chem., Int. Ed.*, 2025, **64**, e202503658.
54 C. Shen, M. Srebro-Hooper, M. Jean, N. Vanthuyne, L. Toupet, J. A. G. Williams, A. R. Torres, A. J. Riives, G. Muller, J. Autschbach and J. Crassous, Synthesis and Chiroptical Properties of Hexa-, Octa-, and Deca-azaborahelicenes: Influence of Helicene Size and of the Number of Boron Atoms, *Chem.–Eur. J.*, 2017, **23**, 407–418.
55 J. Full, S. P. Panchal, J. Götz, A. M. Krause and A. Nowak-Król, Modular Synthesis of Organoboron Helically Chiral Compounds: Cutouts from Extended Helices, *Angew. Chem., Int. Ed.*, 2021, **60**, 4350–4357.
56 F. Full, Q. Wölflick, K. Radacki, H. Braunschweig and A. Nowak-Król, Enhanced Optical Properties of Azaborole Helicenes by Lateral and Helical Extension, *Chem.–Eur. J.*, 2022, **28**, e202202280.
57 J. Full, M. J. Wildervanck, C. Dillmann, S. P. Panchal, D. Volland, F. Full and K. Meerholz, A. Nowak-Król, Impact of Truncation on Optoelectronic Properties of Azaborole Helicenes, *Chem.–Eur. J.*, 2023, **29**, e202302808.
58 F. Full, A. Artigas, K. Wiegand, D. Volland, K. Szkodzińska, Y. Coquerel and A. Nowak-Król, Controllable 1,4-Palladium Aryl to Aryl Migration in Fused Systems—Application to the Synthesis of Azaborole Multihelicenes, *J. Am. Chem. Soc.*, 2024, **146**, 29245–29254.
59 W. D. Petrykowski, N. Vanthuyne, C. Naim, F. Bertocchi, Y. M. Poronik, A. Ciesielski, M. K. Cyrański, F. Terenziani,

D. Jacquemin and D. T. Gryko, Double helicene possessing B–N dative bonds built on 1,4-dihydropyrrolo[3,2-b]pyrrole core, *Chem. Sci.*, 2025, **16**, 8338–8345.

60 V. F. Pais, M. M. Alcaide, R. López-Rodríguez, D. Collado, F. Nájera, E. Pérez-Inestrosa, E. Álvarez, J. M. Lassaletta, R. Fernández, A. Ros and U. Pischel, Strongly Emissive and Photostable Four-Coordinate Organoboron N,C Chelates and Their Use in Fluorescence Microscopy, *Chem.–Eur. J.*, 2015, **21**, 15369–15376.

61 Z. Domínguez, R. López-Rodríguez, E. Álvarez, S. Abbate, G. Longhi, U. Pischel and A. Ros, Azabora[5]helicene Charge-Transfer Dyes Show Efficient and Spectrally Variable Circularly Polarized Luminescence, *Chem.–Eur. J.*, 2018, **24**, 12660–12668.

62 D. L. Crossley, I. A. Cade, E. R. Clark, A. Escande, M. J. Humphries, S. M. King, I. Vitorica-Yrezabal, M. J. Ingleson and M. L. Turner, Enhancing electron affinity and tuning band gap in donor–acceptor organic semiconductors by benzothiadiazole directed C–H borylation, *Chem. Sci.*, 2015, **6**, 5144–5151.

63 A. Haque, R. A. Al-Balushi, P. R. Raithby and M. S. Khan, Recent Advances in π-Conjugated N^C-Chelate Organoboron Materials, *Molecules*, 2020, **25**, 2645.

64 A. C. Murali, P. Nayak and K. Venkatasubbaiah, Recent advances in the synthesis of luminescent tetra-coordinated boron compounds, *Dalton Trans.*, 2022, **51**, 5751–5771.

65 N. Ishida, T. Moriya, T. Goya and M. Murakami, Synthesis of Pyridine−Borane Complexes *via* Electrophilic Aromatic Borylation, *J. Org. Chem.*, 2010, **75**, 8709–8712.

66 E. Vander Donckt, J. Nasielski, J. Greenleaf and J. Birks, Fluorescence of the helicenes, *Chem. Phys. Lett.*, 1968, **2**, 409–410.

67 K. Dhbaibi, L. Favereau, M. Srebro-Hooper, M. Jean, N. Vanthuyne, F. Zinna, B. Jamoussi, L. Di Bari, J. Autschbach and J. Crassous, Exciton coupling in diketopyrrolopyrrole–helicene derivatives leads to red and near-infrared circularly polarized luminescence, *Chem. Sci.*, 2018, **9**, 735–742.

68 R. Bouvier, R. Durand, L. Favereau, M. Srebro-Hooper, V. Dorcet, T. Roisnel, N. Vanthuyne, Y. Vesga, J. Donnelly, F. Hernandez, J. Autschbach, Y. Trolez and J. Crassous, Helicenes Grafted with 1,1,4,4-Tetracyanobutadiene Moieties: π-Helical Push–Pull Systems with Strong Electronic Circular Dichroism and Two-Photon Absorption, *Chem.–Eur. J.*, 2018, **24**, 14484–14494.

69 F. Zhang, E. Michail, F. Saal, A. M. Krause and P. Ravat, Stereospecific Synthesis and Photophysical Properties of Propeller-Shaped C90H48 PAH, *Chem.–Eur. J.*, 2019, **25**, 16241–16245.

70 J. A. Schellman, Circular dichroism and optical rotation, *Chem. Rev.*, 1975, **75**, 323–331.

71 H. Kubo, T. Hirose, T. Nakashima, T. Kawai, J.-y. Hasegawa and K. Matsuda, Tuning Transition Electric and Magnetic Dipole Moments: [7]Helicenes Showing Intense Circularly Polarized Luminescence, *J. Phys. Chem. Lett.*, 2021, **12**, 686–695.

72 (*a*) CCDC 2488475: Experimental Crystal Structure Determination, 2026, DOI: 10.5517/ccdc.csd.cc2pjgd3; (*b*) CCDC 2488477: Experimental Crystal Structure Determination, 2026, DOI: 10.5517/ccdc.csd.cc2pjgg5.